Copy 9
C. Bailey

November 1948

PRESSURE DISTRIBUTION TESTS ON A CIRCULAR CYLINDER ALIGNED LONGITUDINALLY WITH A FREE STREAM AT MACH NUMBER 1.93.

EMB-11

NoJ 48

PREPARED BY A. H. Kelly

APPROVED BY F. W. Ross

AERONAUTICAL RESEARCH CENTER

WILLOW RUN AIRPORT YPSILANTI, MICHIGAN

TABLE OF CONTENTS

INTRODUCTION

The purpose of this report is to present the results of supersonic wind tunnel tests on a cylindrical pressure model aligned longitudinally with the free stream, at various angles of attack.

The cylindrical model (1.5" in diameter and 3.75" long) equipped with 47 pressure orifices, was tested in the U.M.E.R.I. (8" x 13") supersonic wind tunnel at a Mach number of 1.93. Pressure measurements only were made on the model.

SUMMARY

Supersonic wind tunnel tests were made on a cylindrical pressure model aligned longitudinally with the freestream at various angles of attack. The pressures at various positions on the longitudinal surface and over the face of the model were recorded, (no readings were taken for the base of the model) and Schlieren photographs were taken.

From these pressures the values of C_p, C_N, F_N, C.P$_s$. C_{F_f}, F_f, C.P$_f$., C_{M_T} and M_T were calculated, with α used as a parameter and the results presented in graphical form.

From the graphs and Schlieren photographs several conclusions and observations can be made.

1. The major portion of the normal force was due to the longitudinal position of the shock wave originating on the surface of the model. That is, the shock wave was further aft on the top of the model. See Figure 4.

2. The variations of C_N, C.P$_s$., C_{M_T} and C.P$_f$ with α are linear (Figures 14, 15, 16, and 20).

3. Variation of the force on the face of the model with α was too small to be evaluated. The value of C_{F_f} was .388 (F_f = 3.63 lb.). The C.P. of this force, however, moved downward 1.3% of the radius per degree increase of α. This C.P$_f$. movement caused the force on the face to account for approximately 6% of the total moment about the center of the face of the model (Figure 16).

Symbols

A = Face area, x in^2

C_{M_T} = Total moment coefficient about center of face of model = $\frac{M_T}{qAd}$

c_N = Longitudinal station normal force coefficient

C_N = Total normal force coefficient

C_p = Pressure coefficient = $\frac{p - p_a}{q}$

C,P_f = Center of pressure on face of cylinder in % of radius

C.P. = Center of Pressure on longitudinal axis of cylinder in % of model length

d = Diameter of cylinder, in.

F_f = Total force on face of model, lb.

= Nose pressure drag on model

F_n = Normal force on cylinder, Lb. i.e. normal to xy plane (See Figure 1)

l = Length of cylinder, in.

M = Moment about center of face due to F_N, in. lb.

M_f = Moment about center of face due to F_f, in. lb.

M_T = Total moment about center of face = $M_s + M_f$, in. lb.

p = Fluid pressure, p.s.i.

p_a = Ambient pressure, p.s.i.

q = Free stream dynamic pressure, p.s.i.

r = Radius of cylinder, in.

X,Y.Z ; Right hand cartesian coordinate system. See Figure 1

ρ = Radius on face, in.

α = Angle of attack

ϕ = Angle in yz plane measured counterclockwise from positive Z Axis radians. (See Figure 1)

DESCRIPTION OF MODEL

The model used in these tests, (Figure 2), was a stainless steel cylinder 1.50" in diameter and 3.75" long. The model was supported from the rear by a hollow steel sting. There were four rows, located 90° apart, of seven orifices each on the longitudinal surface of the model. The first orifice in each row was .30" aft of the face of the cylinder, and the orifice spacing was .50". There was an orifice in the center of the face, a ring of six orifices 60° apart at ρ = .30", and a ring of twelve orifices 30° apart at ρ = .60". Thus there were 28 orifices on the longitudinal surface of the model, and 10 on its face; a total of 47. There were no pressure orifices on the base of the model. Each orifice was .0225" in diameter. 1/16" O.D. by .028" I.D. copper tubing lead from the orifices through the sting, the floor of the wind tunnel, and then to the manometer board.

TEST PROCEDURE

The model was installed in the U.M.E.R.I. supersonic wind tunnel, with $\phi = 0$, and runs were made at 2° increments of α from $\alpha = -10°$ to $\alpha = +10°$. Then the model was rotated 45° ($\phi = \pi/4$), and runs were made at the angles of attack listed above. This procedure provided four readings for each surface orifice position.

At least two runs were made at each position. Two manometer board photographs, and one Schlieren photograph, were taken at each position. Figures 3 and 4 are representative Schlieren photographs. The Mach number for all runs was 1.93.

REDUCTION OF DATA

The pressure distribution data was reduced to force and moment coefficients, and the centers of pressure were located by graphical methods. A brief explanation of these methods is given in Appendix A.

DISCUSSION

The following discussion is an attempt to describe, with the aid of the test data and physical reasoning, the flow phenomena which are shown on the Schlieren photographs. There being little basic theory or previous experimentation applicable to supersonic flow over a cylindrical body aligned longitudinally to the flow, the two tools named above are the only ones available at present for use in explaining the flow in question.

To facilitate the description, constant reference will be made to Figures 3A and 4A which are facsimiles of the two Schlieren photographs presented in figures three and four.

In order to adequately explain the flow one can first determine the extent of the subsonic region which occurs behind the detached shock wave. It is reasonable to assume that the angle of the detached shock, and the Mach number immediately behind it are the same as those which can be theoretically calculated for a two dimensional shock wave occuring with a free stream Mach number of 1.93. Utilizing this assumption, reference (1) yields a shock angle of 61° for compression through and oblique shock wave from a Mach number of 1.93 to a Mach number of one. Thus the "sonic" point (point 3) on the detached shock wave is determined. The shock wave which originates on the longitudinal surface of the model comes into play in the determination of the extent of the subsonic region aft of the detached shock. It will be shown that the existence of this second shock wave requires that there be a region of separation over the foremost portion of the cylindrical surface, and that this separated region must necessarily be an integral part of the subsonic regime.

The flow is, of course, supersonic and parallel to the model behind the second shock wave. Thus the surface of the model forward of shock "C" cannot be part of the flow boundary. A feasable flow boundary ahead of the shock is a region of separated flow or near-stagnant air. Such a region, labled "D", is visable on the Schlieren photographs. This region originates above the edge of the face of the model, point 1, and curves over to the intersection, at point 2, of shock wave "C" and the surface of the model.

Referring to Figure 4, a weak expansion region is visible originating at point 1, therefore it is concluded that the flow must be supersonic at this point. Though the expansion region at zero angle of attack is not shown to be of the simple type, it is believed that point

1 is a point near the subsonic-supersonic boundary line in this case as well as in the case of an angle of attack different from zero.

Having established the probable extent of the subsonic and "stagnant" air regions, the remainder of the flow over the cylinder can be qualitatively explained. The existence of the expansion region, "E", is shown by the light colored area on the Schlieren photographs, which indicates a negative density gradient. At point 4 on the detached shock wave there is a marked decrease of the slope of the shock. This indicated the intersection of an expansion region with the shock wave, therefore point 4 is considered to be the intersection of the strongest portion of the expansion region, "E", with the shock wave.

The general flow direction is now determined through the initial shock wave and the expansion region. Upon emerging from the expansion region the flow is inclined to the surface of the model. Thus the shock wave from the surface of the model is required to satisfy the boundary condition that the flow be parallel to the model aft of the region of more or less stagnant air.

The flow over the model at an angle of attack is of the same nature as that at zero angle of attack. That is, there is a subsonic and stagnation region near the front of the model, and the shock wave originating on the surface of the model is present in both cases. The difference between the two cases lies in the location and strength of the shock waves, and the variation in pressure distribution. These differences are shown in the graphs.

Figures 5, 10, and 17 exhibit the axial symmetry of the flow at zero angle of attack. Figures 5 (C_p vs ϕ) shows that the pressure coefficient is not a function of ϕ at $\alpha = 0$, and figures 6 through 9 show the variation of C_p with ϕ at various axial positions, with an angle of attack of 10°.

Figure 17 shows the symmetry of pressure distribution over the face of the model at zero angle of attack, while the following two figures show the destruction of this symmetry as the angle of attack increases.

The variation in normal force coefficient with angle of attack was found to be 0.043 per degree, but the variation in the force on the face of the model was too small to be calculated.

The variation, in position and strength, of the shock wave which

originates on the surface of the model is shown in figures 11 and 12. From these two figures together with figure 13, it is apparent that the major portion of the normal force on the model is due to the variation, with ϕ, of the axial position of the shock wave.

A comparision between theory and experiment is afforded by the pressure reading at the center of the face of the model, at zero angle of attack. It is reasonable to assume that this reading is the total head behind a normal shock wave. One dimension supersonic flow theory yields the following results (Reference 2):

$$\frac{\frac{P_o'}{P_o}}{\frac{P_a}{P_o}} = \frac{.7535}{.1425} = 5.29 = \frac{P_o'}{P_a}$$

The value of this ration from the tests was 5.27.

APPENDIX A

Method of Data Reduction

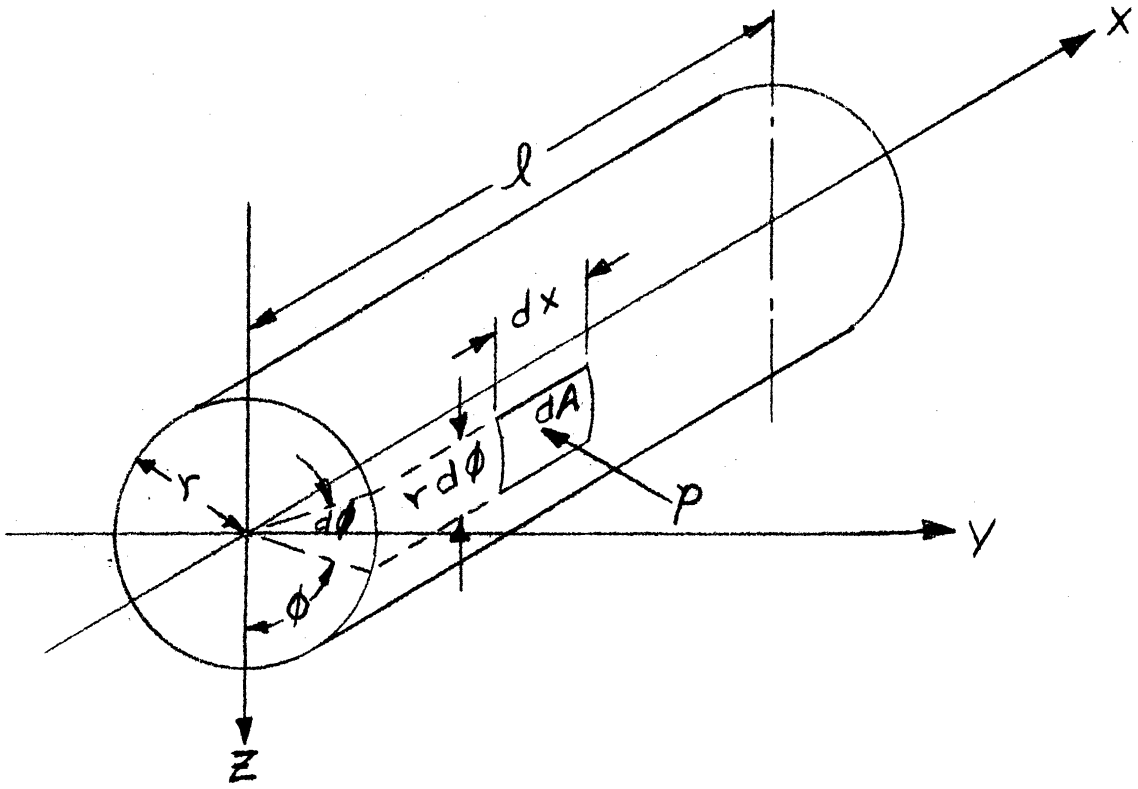

Coordinate System

Figure 1

Using Figure 1, and assuming symmetrical flow about the XZ plane, the following equations may be written:

1. $$C_N = \frac{2r}{A} \int_0 \int_0^{\pi} C_p \cos\phi \, d\phi \, dx$$

2. $$c_N = \frac{2r}{A} \int_0^{\pi} C_p \cos\phi \, d\phi$$

3. $$\bar{X} = \frac{\frac{2r}{A} \int_0 \int_0^{\pi} C_p \cos\phi \; x \, d\phi \, dx}{C_N}$$

4. $$F_f = 2P_a \int_0^{r} \int_0^{\pi} \frac{P}{P_a} \rho \, d\phi \, d\rho$$

5. $$\bar{Z} = \frac{2P_a \int_0^{r} \int_0^{\pi} \frac{P}{P_a} \cos\phi \, \rho^2 \, d\phi \, d\rho}{F_f}$$

6. $M_T = F_N \bar{X} + F_f \bar{Z}$

These equations were integrated graphically, with the exception of equation 6, to obtain the data presented in this report.

REFERENCES

1. "Notes and Tables For Use in the Analysis of Supersonic Flow" N.A.C.A. TN 1428

2. "Tables and Charts of Flow Parameters Across Oblique Shocks" N.A.C.A. TN 1673

LIST OF FIGURES

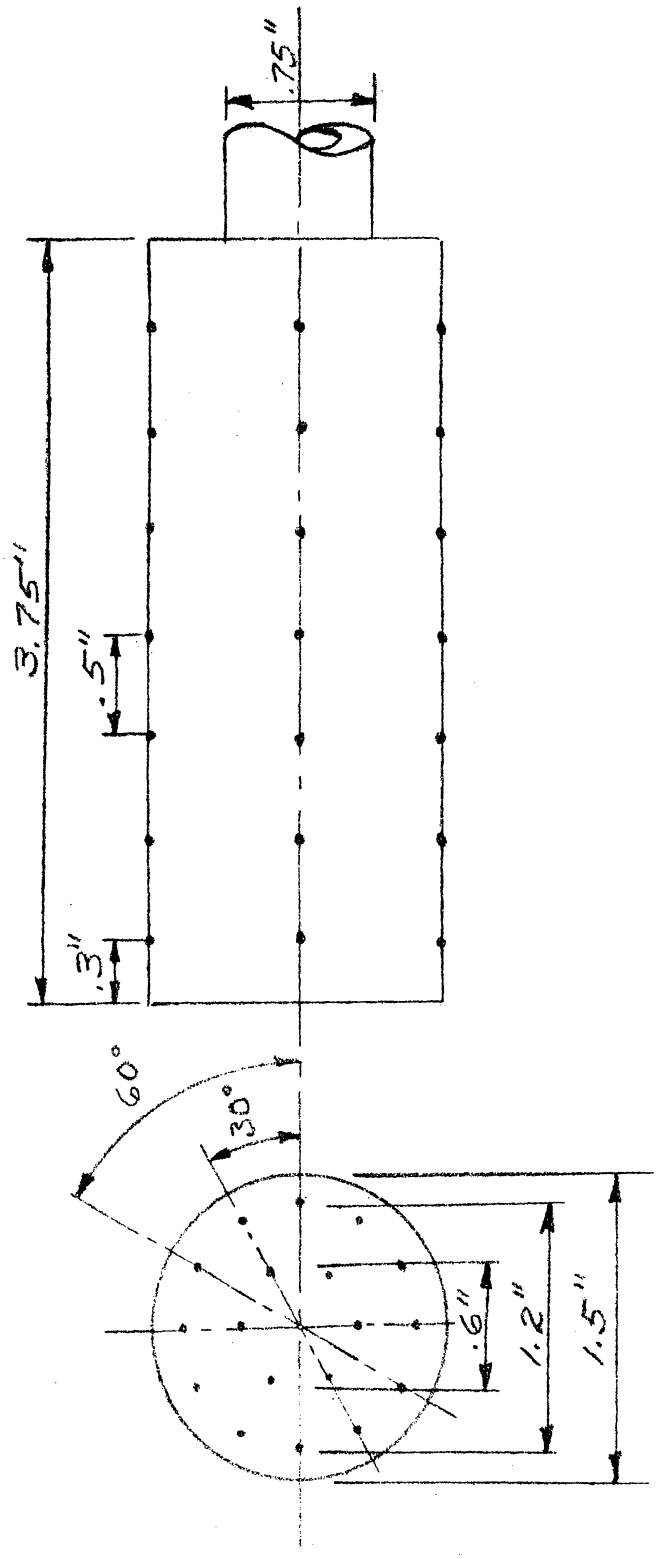

FIGURE 2

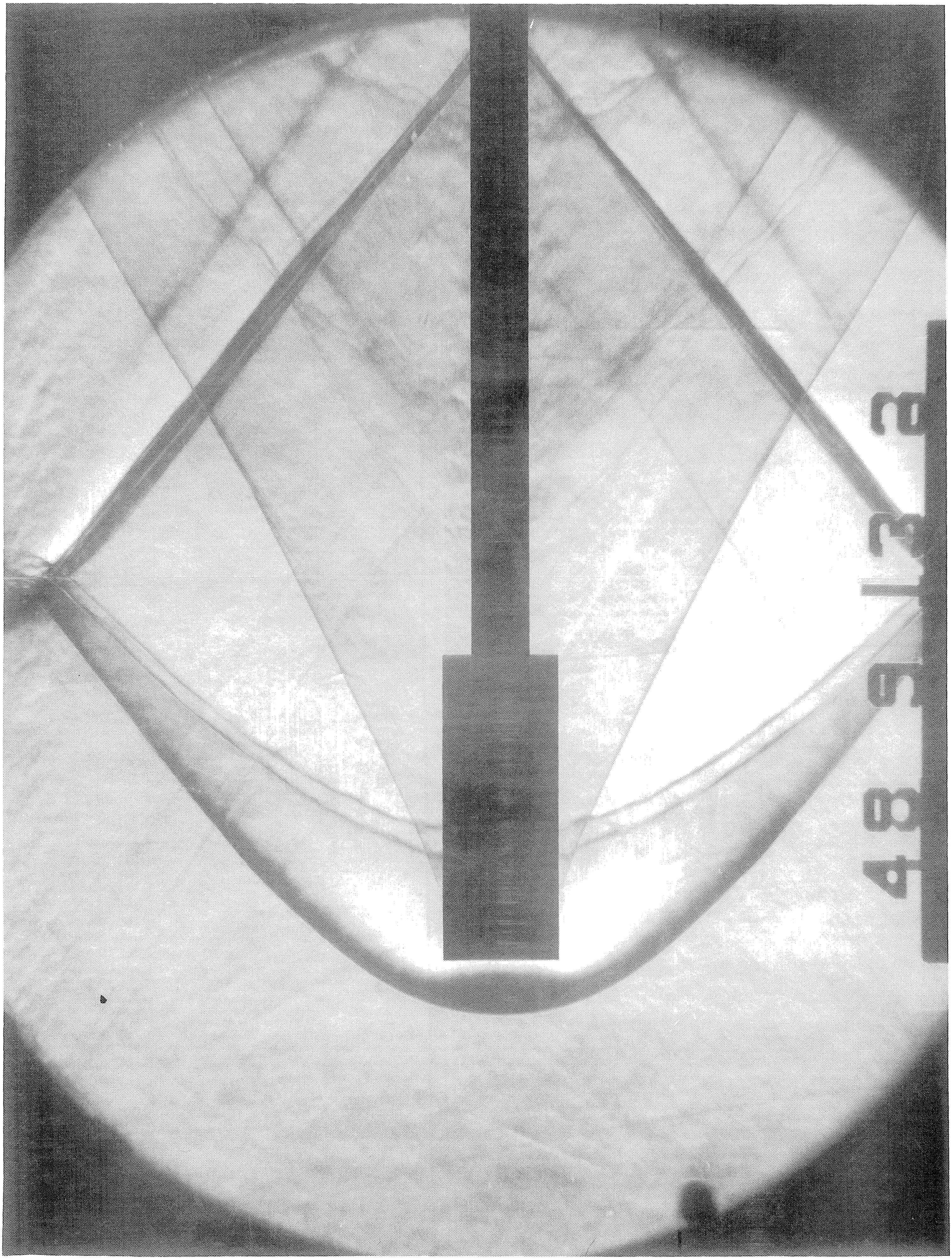

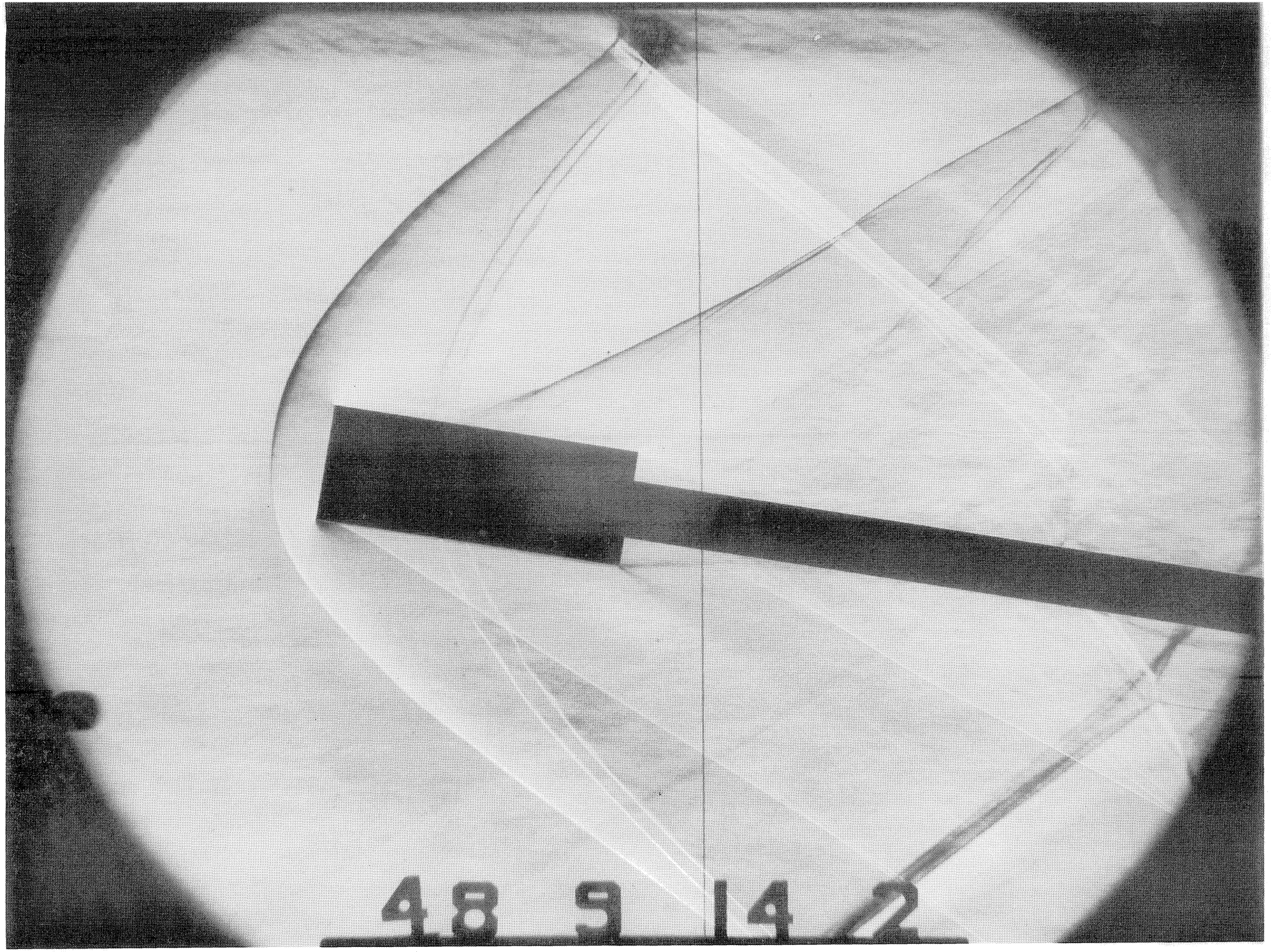
48 9 14 2

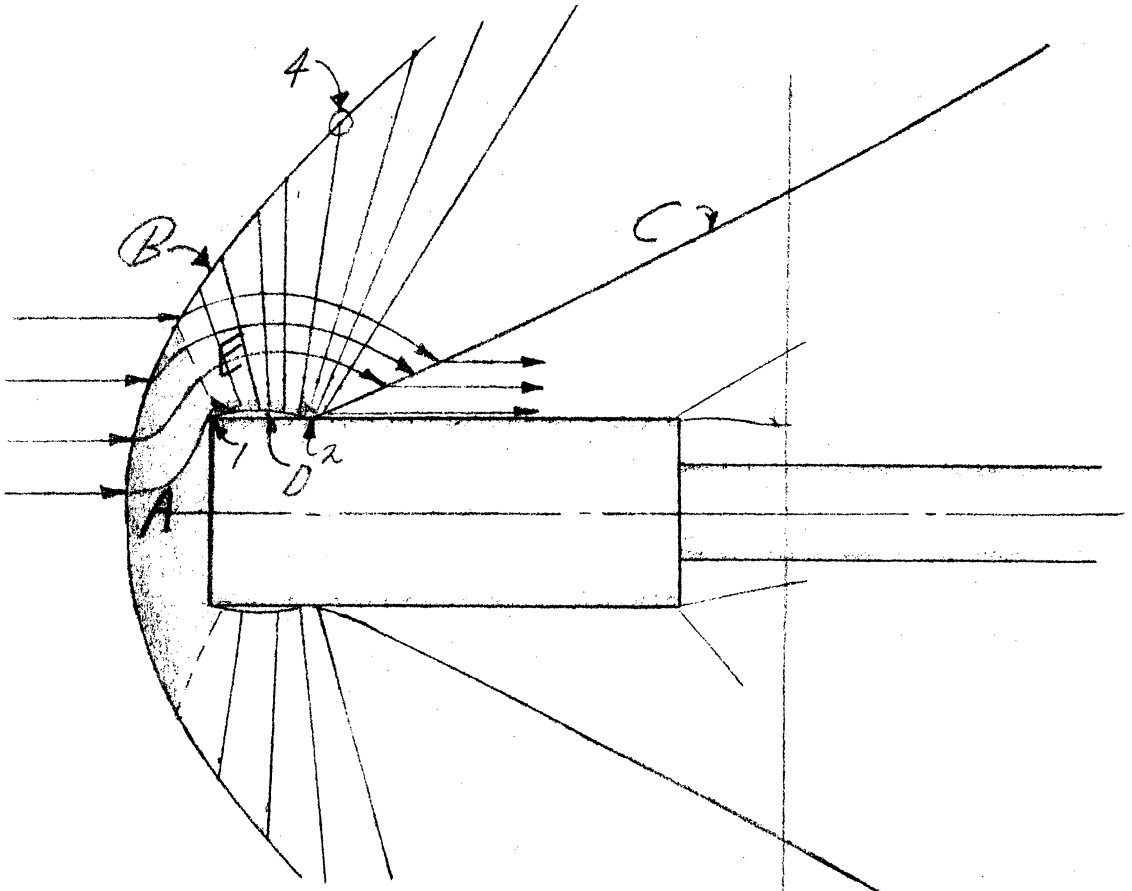

FIGURE 3a

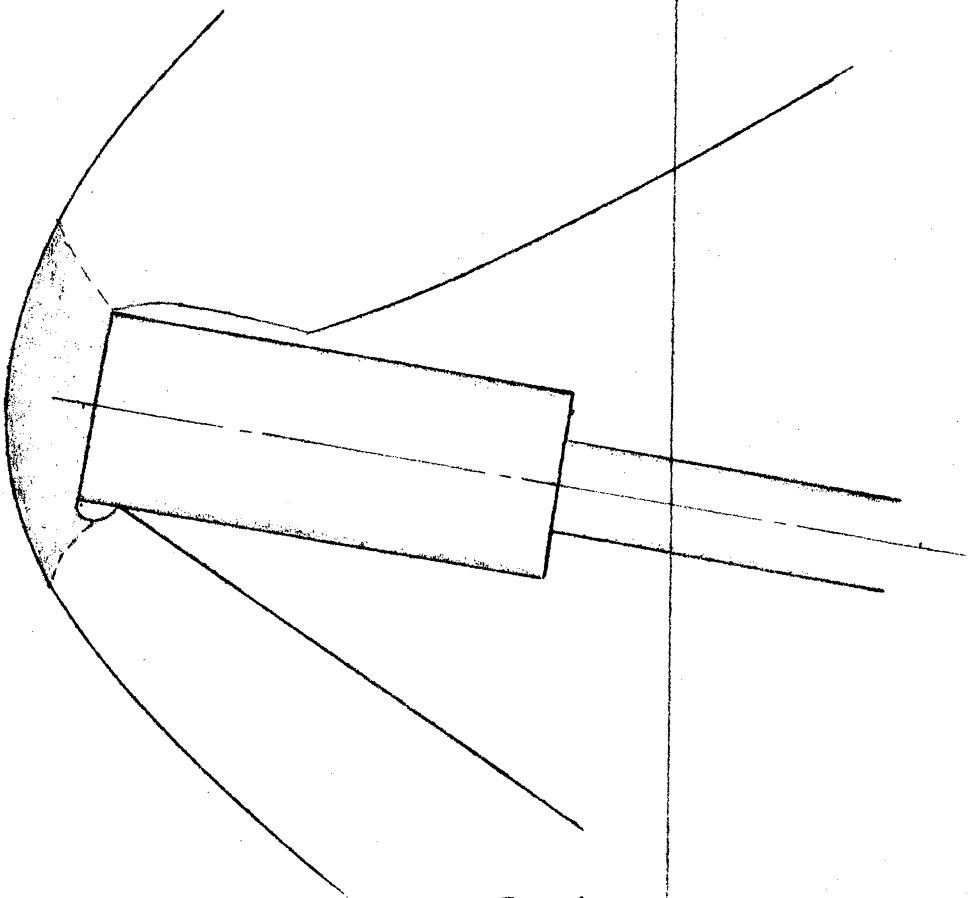

FIGURE 4a

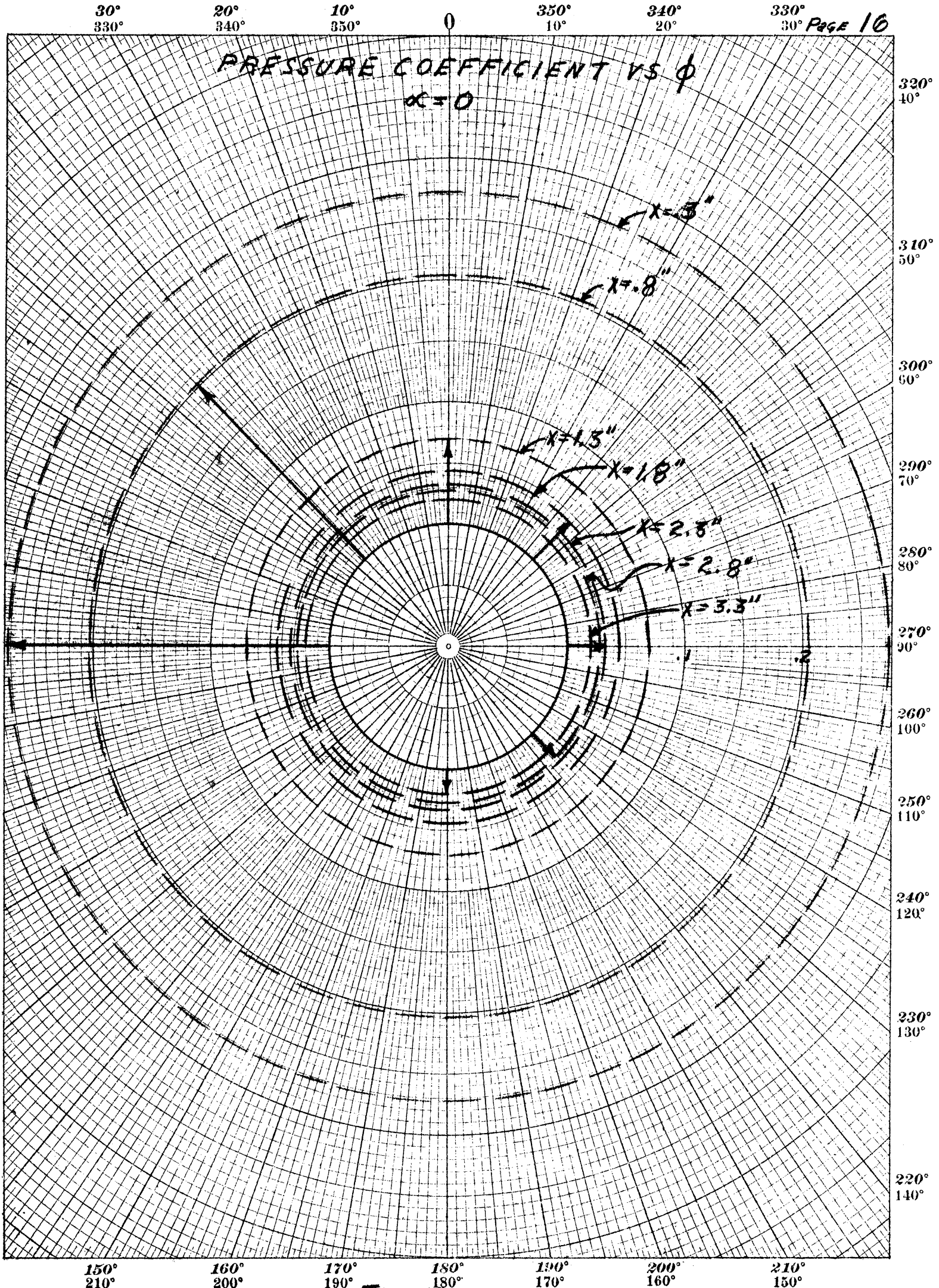
PRESSURE COEFFICIENT VS φ
α = 0
x = .3"
x = .8"
x = 1.3"
x = 1.8"
x = 2.3"
x = 2.8"
x = 3.3"
.1
.2
0
30° 330°
20° 340°
10° 350°
350° 10°
340° 20°
330° 30°
320° 40°
310° 50°
300° 60°
290° 70°
280° 80°
270° 90°
260° 100°
250° 110°
240° 120°
230° 130°
220° 140°
150° 210°
160° 200°
170° 190°
180° 180°
190° 170°
200° 160°
210° 150°

Fig 5

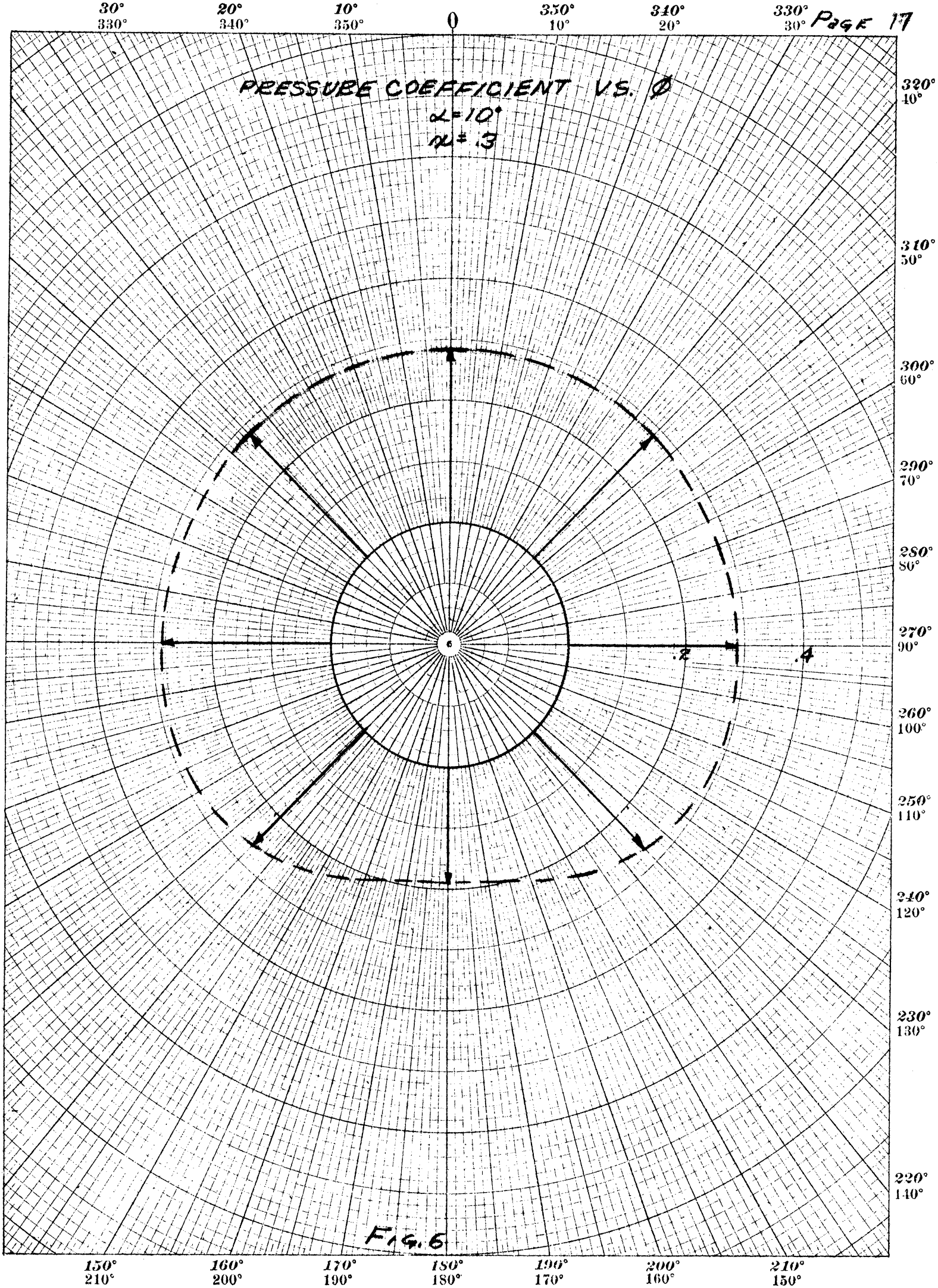
PRESSURE COEFFICIENT VS. Ø
α = 10°
μ = .3
30° 330°
20° 340°
10° 350°
0
350° 10°
340° 20°
330° 30°
320° 40°
310° 50°
300° 60°
290° 70°
280° 80°
270° 90°
260° 100°
250° 110°
240° 120°
230° 130°
220° 140°
.2
.4
150° 210°
160° 200°
170° 190°
180° 180°
190° 170°
200° 160°
210° 150°

FIG. 6

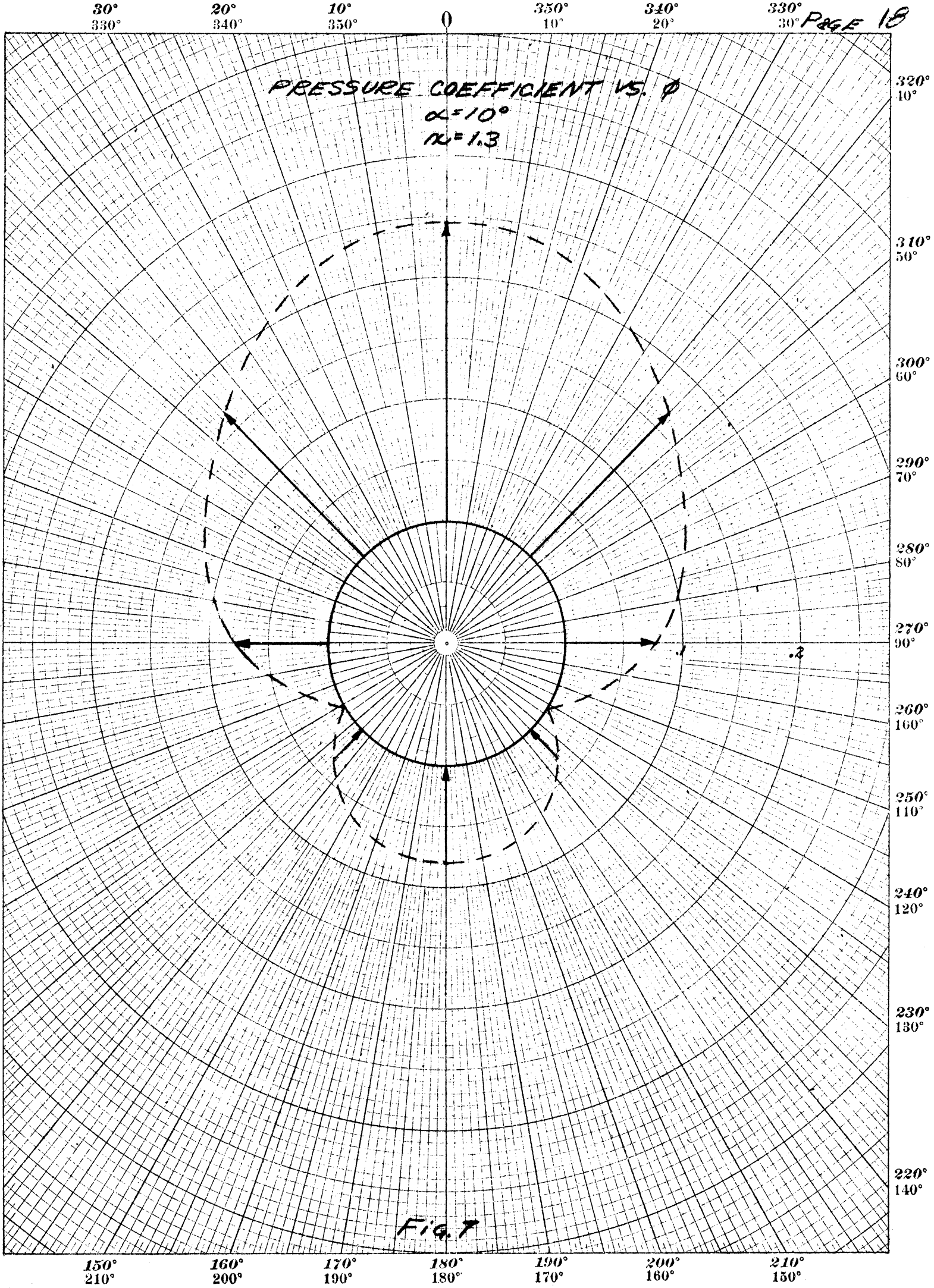
PRESSURE COEFFICIENT VS. Ø
α=10°
M=1.3
30° 330°
20° 340°
10° 350°
0
350° 10°
340° 20°
330° 30°
320° 40°
310° 50°
300° 60°
290° 70°
280° 80°
270° 90°
260° 100°
250° 110°
240° 120°
230° 130°
220° 140°
150° 210°
160° 200°
170° 190°
180°
190° 170°
200° 160°
210° 150°
.2
1

Fig. 7

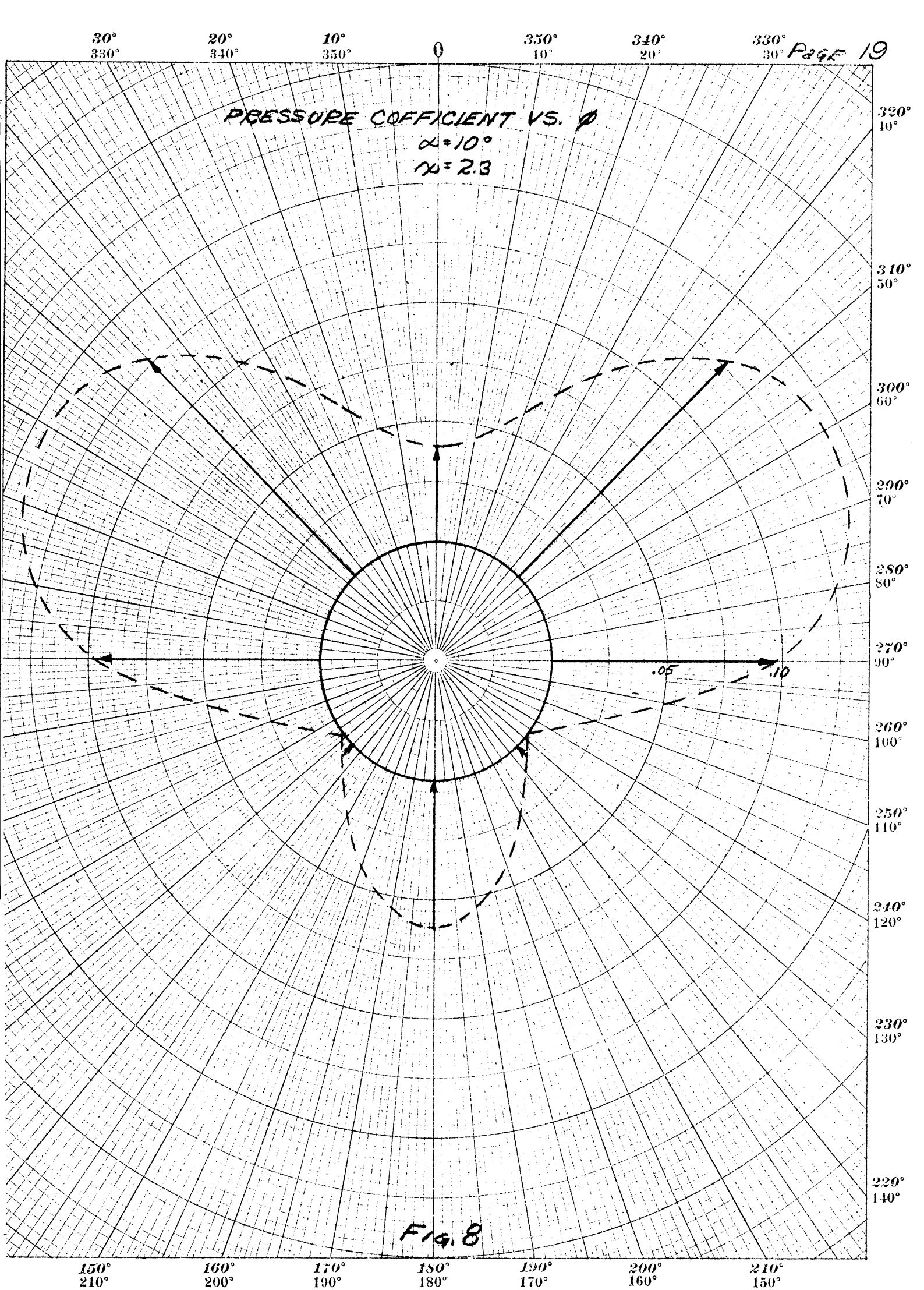
PRESSURE COFFICIENT VS. ∅
α=10°
M=2.3
30° 330°
20° 340°
10° 350°
0
350° 10°
340° 20°
330° 30°
320° 40°
310° 50°
300° 60°
290° 70°
280° 80°
270° 90°
260° 100°
250° 110°
240° 120°
230° 130°
220° 140°
.05
.10
150° 210°
160° 200°
170° 190°
180°
190° 170°
200° 160°
210° 150°

Fig. 8

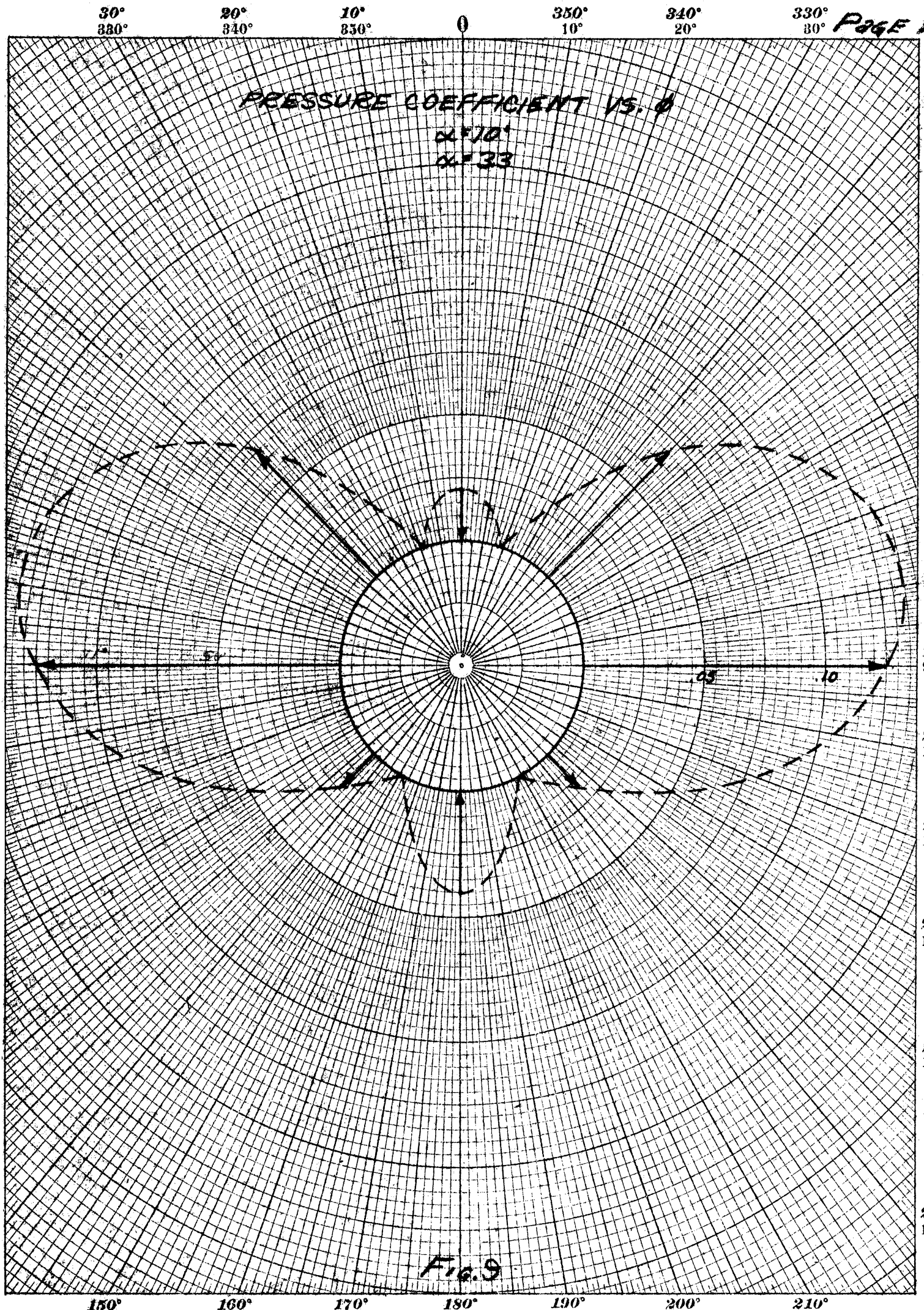
PRESSURE COEFFICIENT VS. ϕ
α = 10°
α = 33
30° 330°
20° 340°
10° 350°
0
350° 10°
340° 20°
330° 30°
320° 40°
310° 50°
300° 60°
290° 70°
280° 80°
270° 90°
260° 100°
250° 110°
240° 120°
230° 130°
220° 140°
150° 210°
160° 200°
170° 190°
180° 180°
190° 170°
200° 160°
210° 150°
.5
1.0

Fig. 9

PRESSURE COEFFICIENT VS. AXIAL DISTANCE

$\alpha = 0°$

FIG. 10

PRESSURE COEFFICIENT VS. AXIAL DISTANCE

$\alpha = 6°$

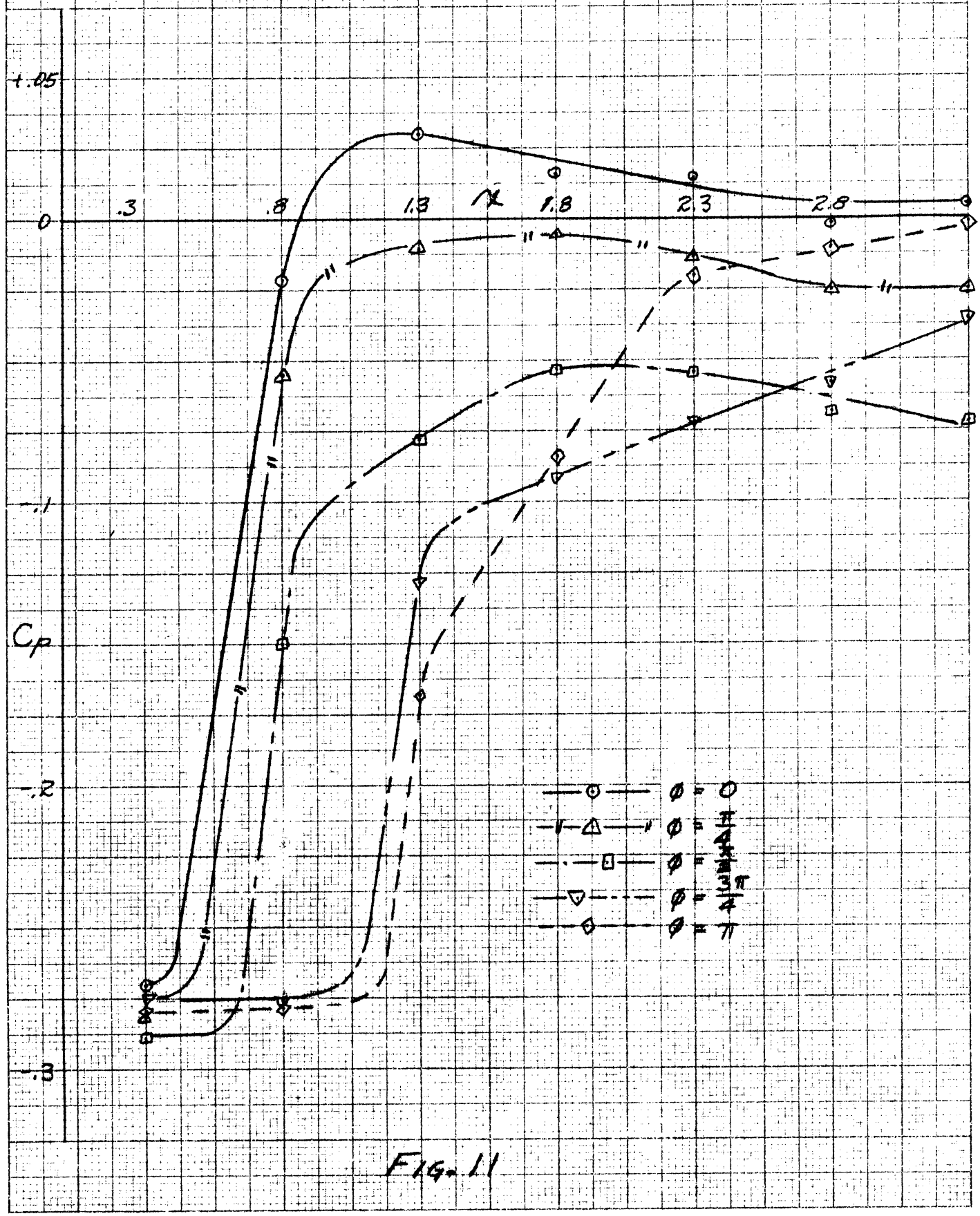

Fig. 11

PRESSURE COEFFICIENT VS. AXIAL DISTANCE

$\alpha = 10°$

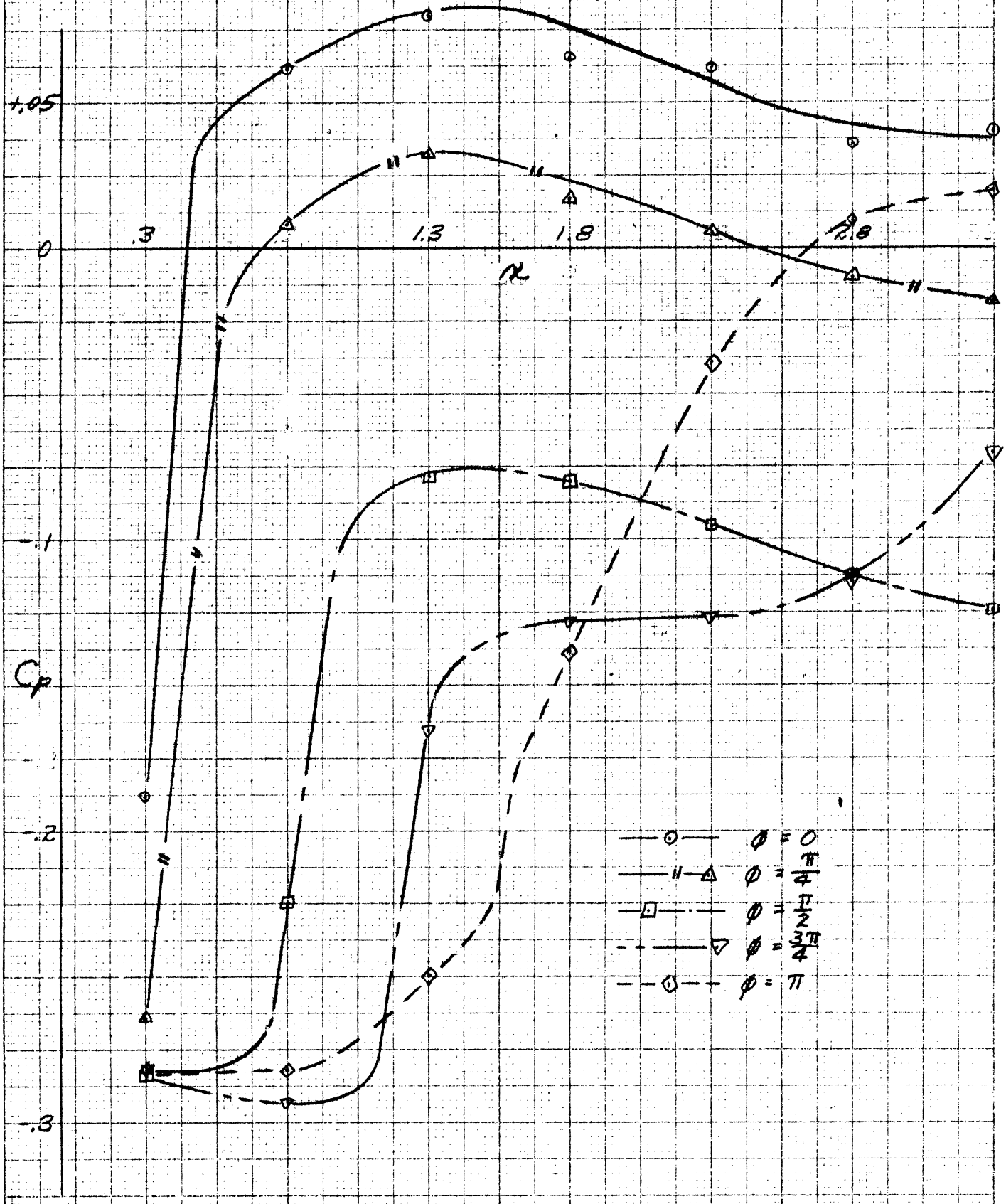

FIG. 12

SECTION NORMAL FORCE COEFFICIENT VS. AXIAL DISTANCE

$\alpha = 10°$

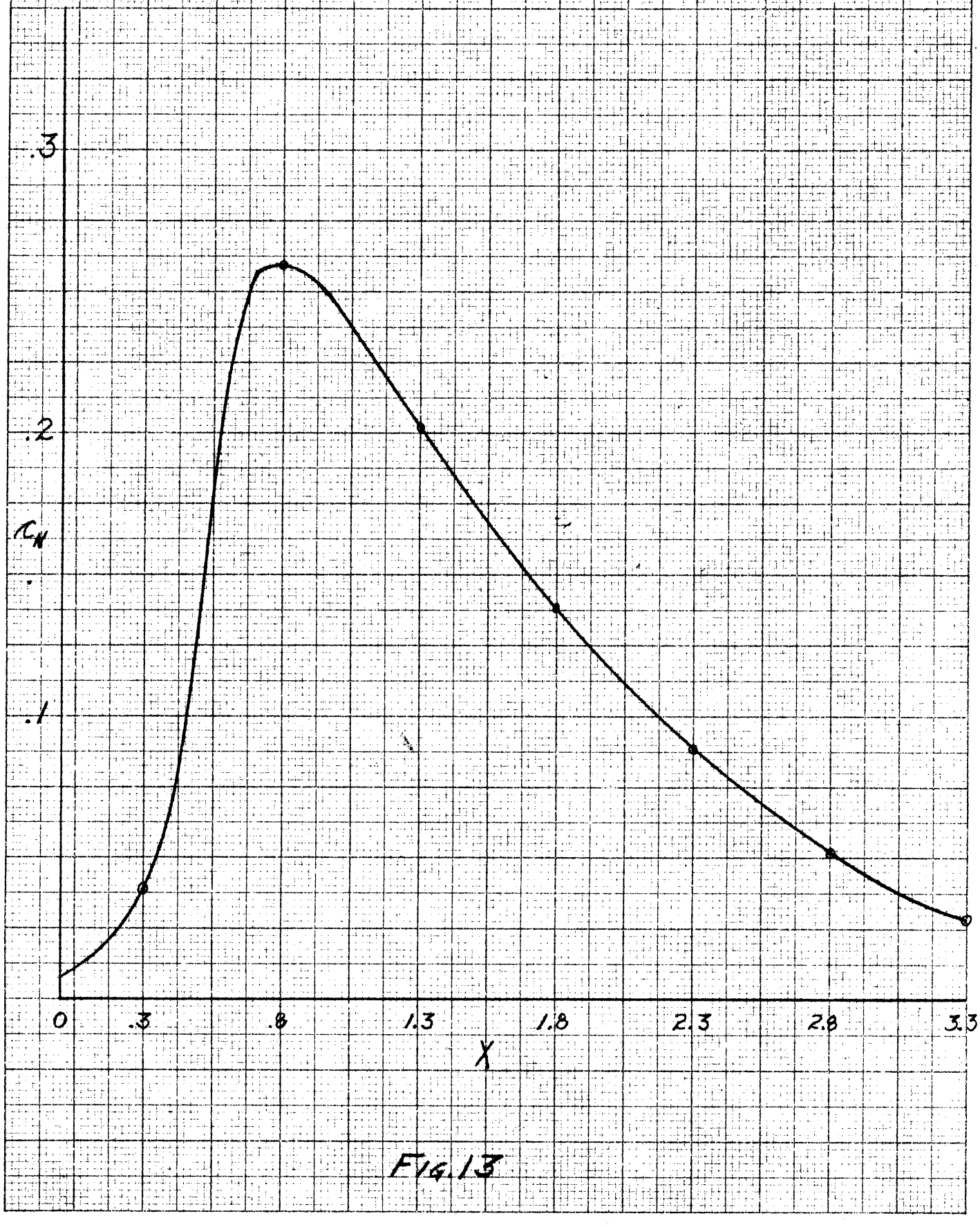

FIG. 13

NORMAL FORCE COEFFICIENT
VS. ANGLE OF ATTACK

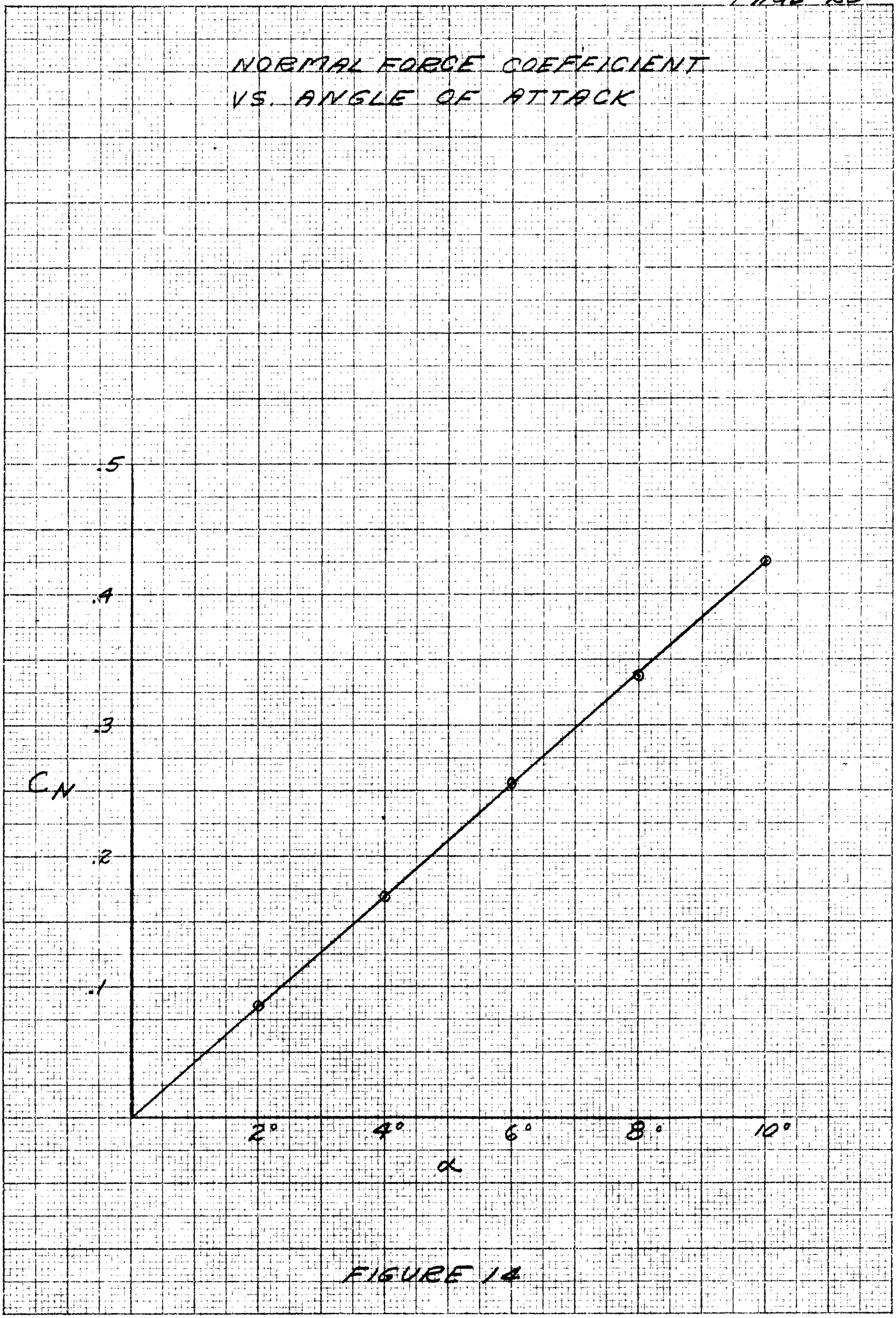

FIGURE 14

CENTER OF PRESSURE IN PERCENT OF LENGTH FROM FACE OF MODEL VS. ANGLE OF ATTACK

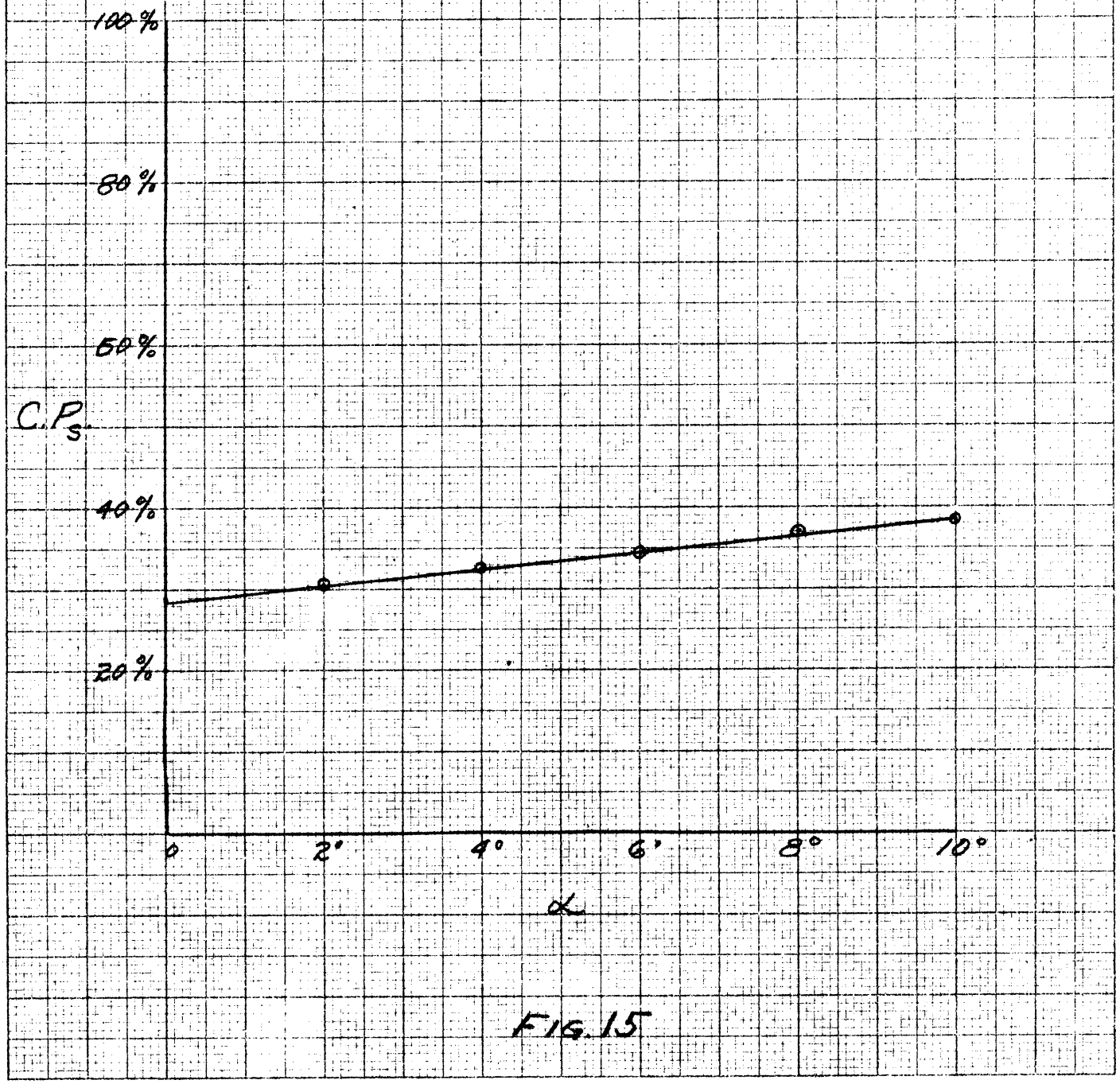

FIG. 15

TOTAL MOMENT COEFFICIENT
(ABOUT THE CENTER OF THE FACE OF THE MODEL)
VS. ANGLE OF ATTACK

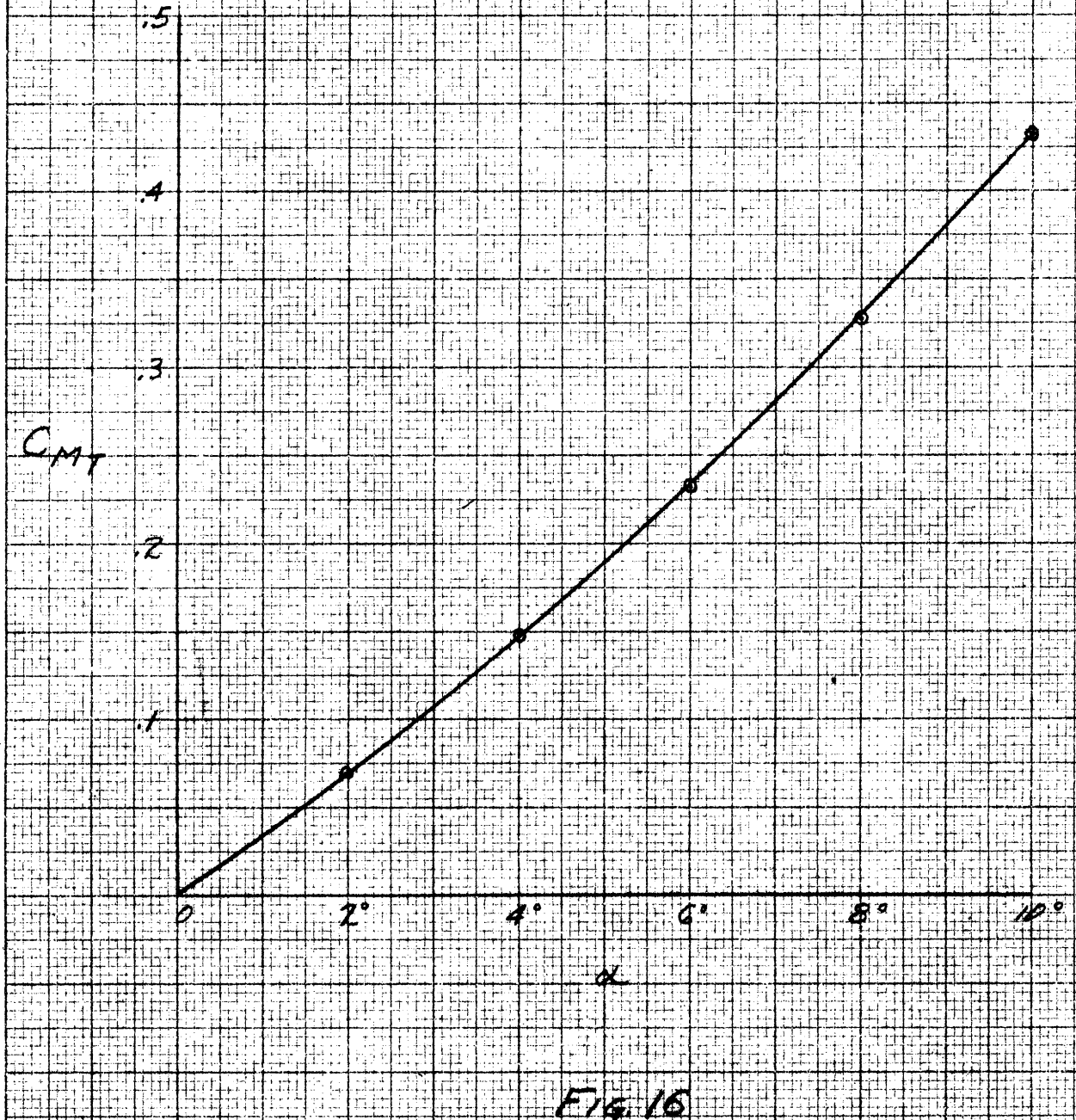

FIG. 16

PRESSURE DISTRIBUTION ON FACE OF MODEL

$\frac{P}{P_0}$ VS. ORIFICE POSITION

$\alpha = 0°$

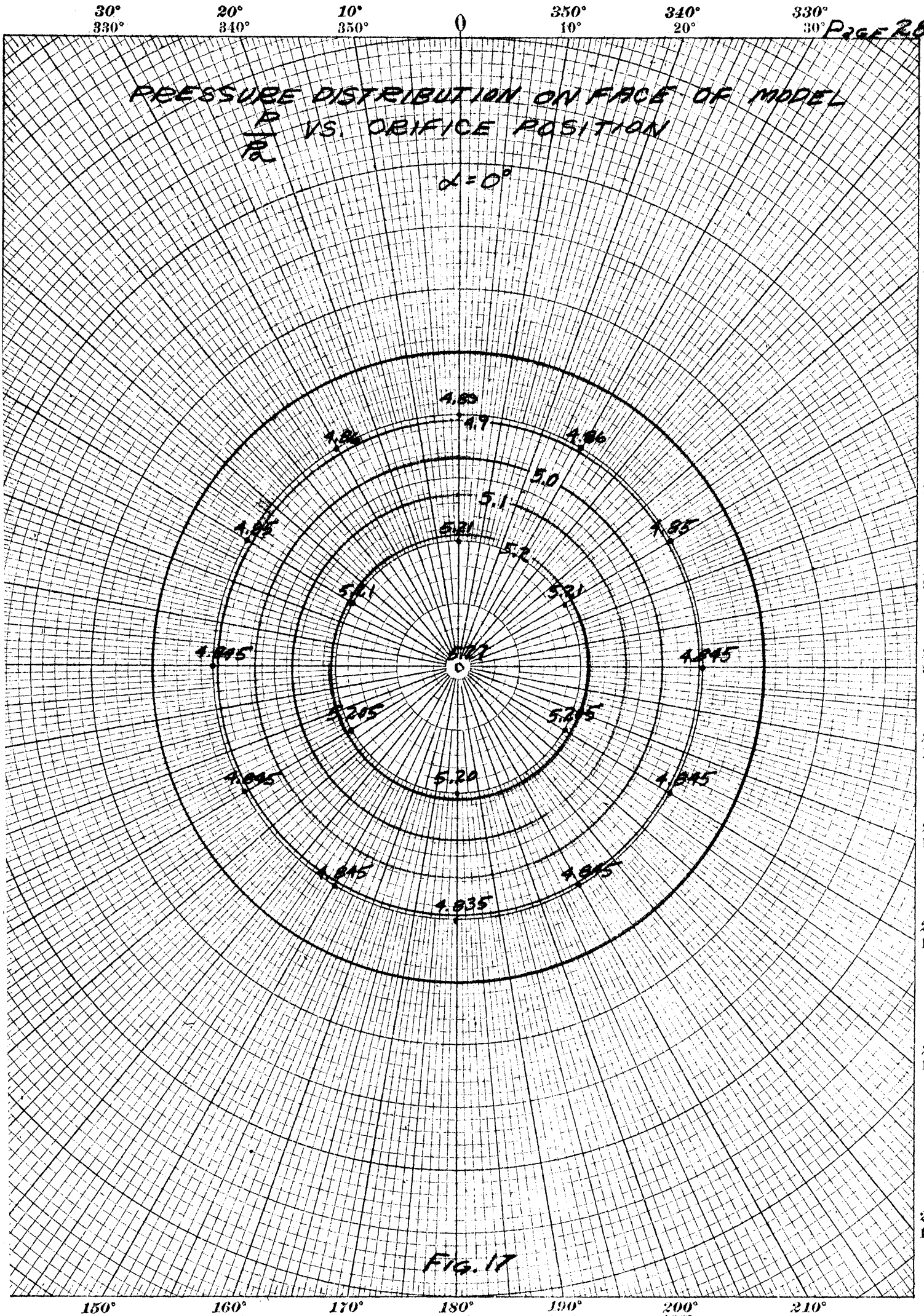

FIG. 17

PRESSURE DISTRIBUTION ON FACE OF MODEL

$\frac{P}{P_{\infty}}$ VS. ORIFICE POSITION

$\alpha = 6°$

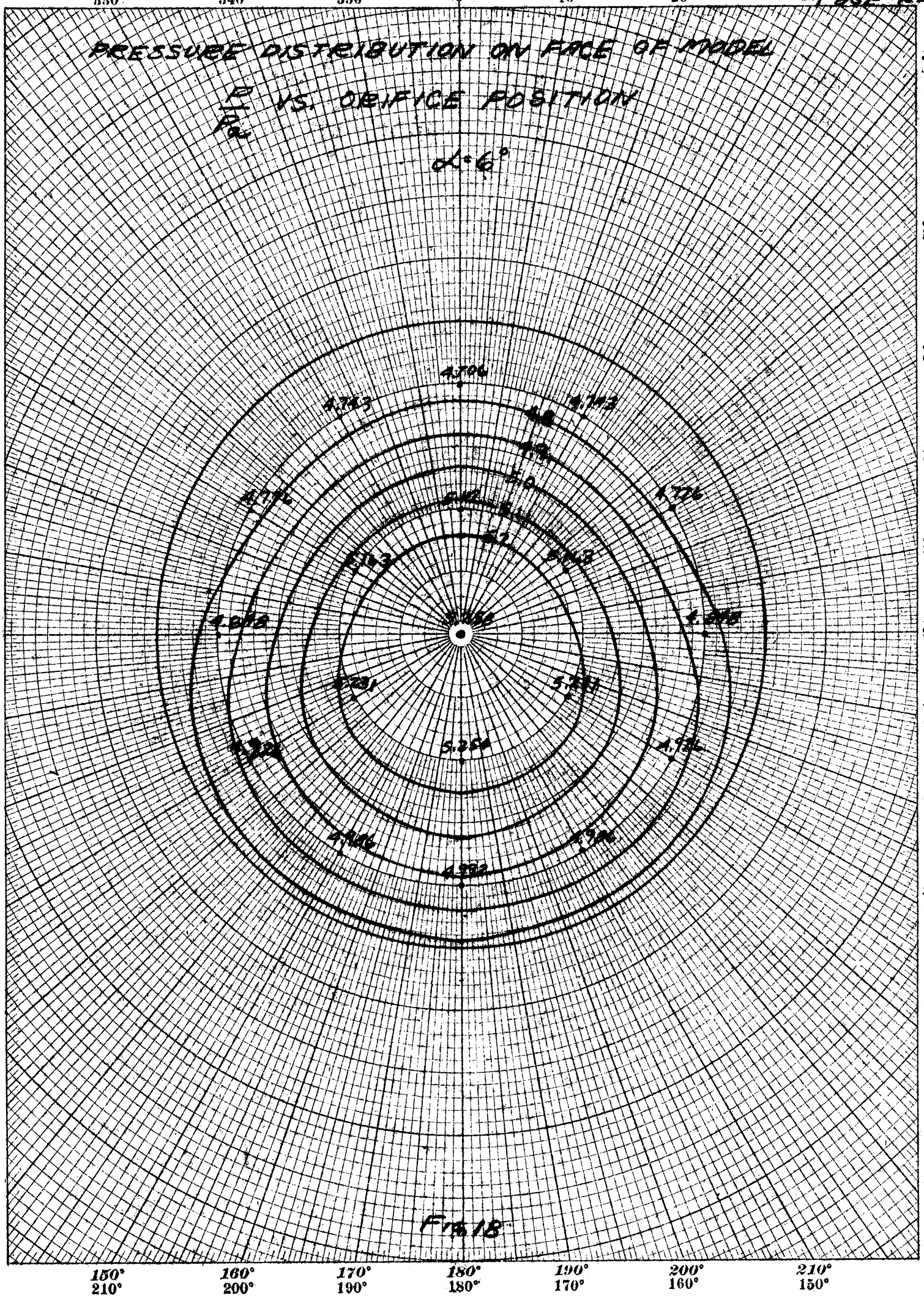

FIG 18

PRESSURE DISTRIBUTION ON FACE OF MODEL

$\frac{P}{P_2}$ VS ORIFICE POSITION

$\alpha = 10°$

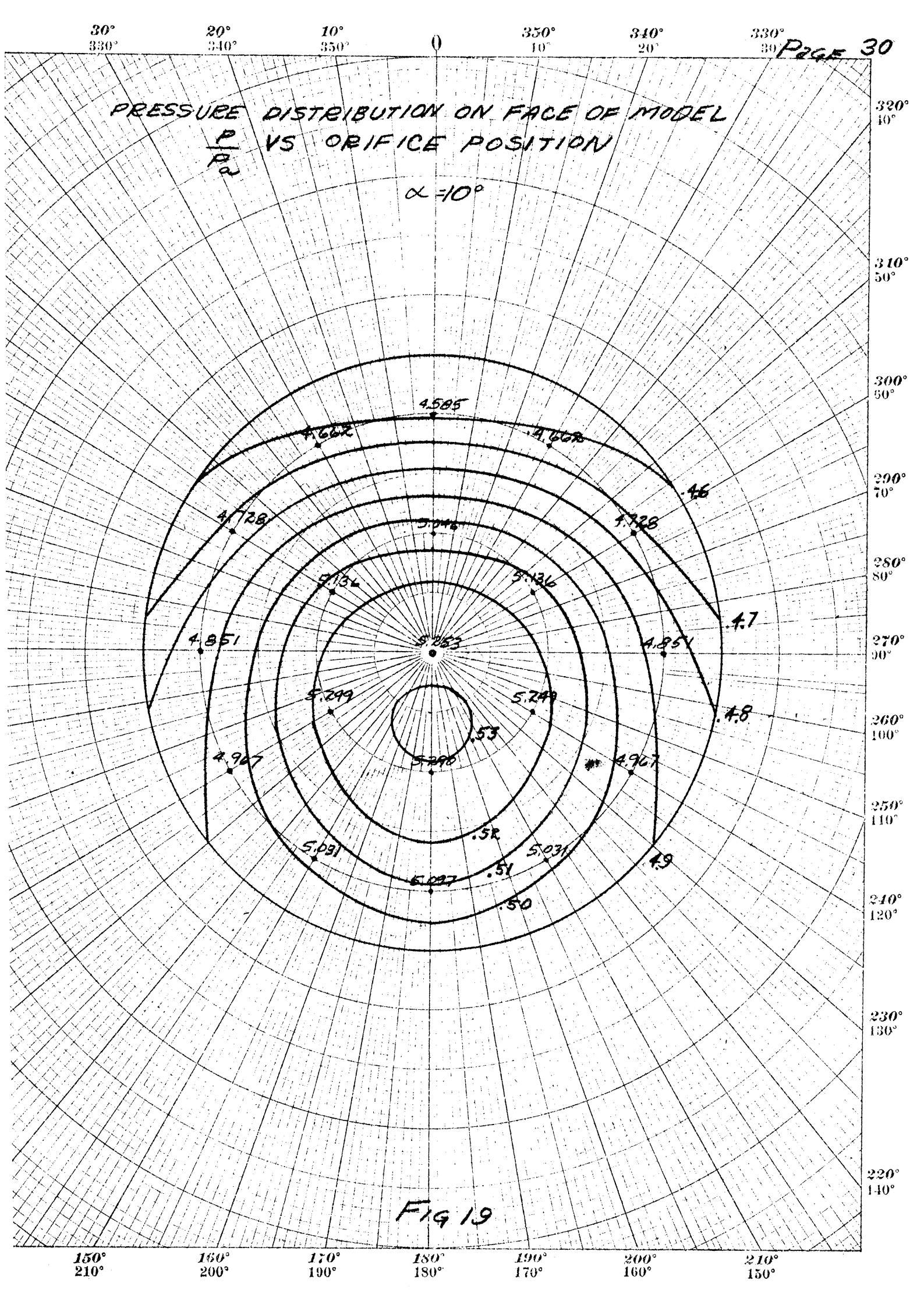

FIG 19

CENTER OF PRESSURE ON FACE OF MODEL
IN PERCENT OF RADIUS VS. ANGLE OF ATTACK

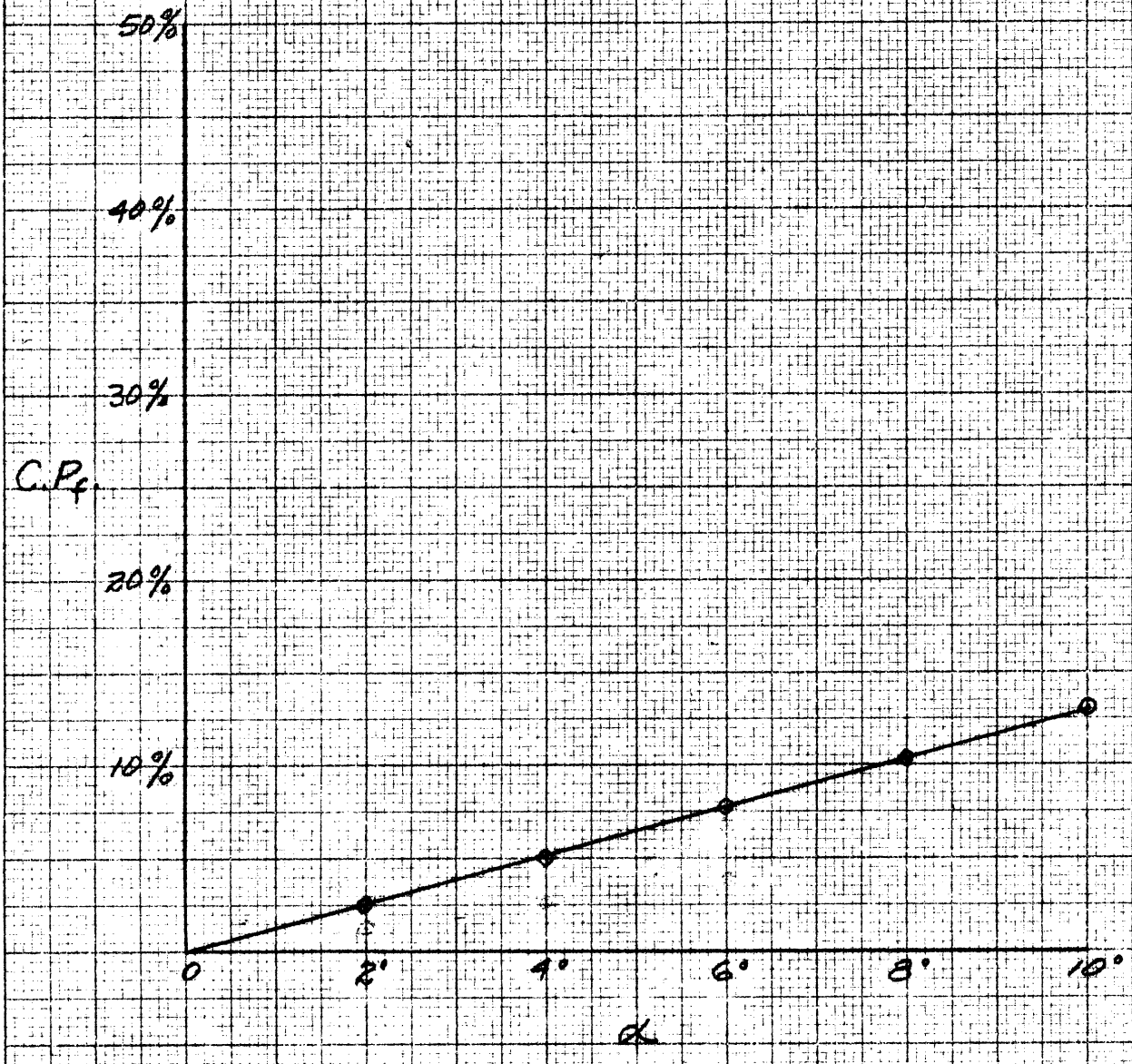

FIG. 20